

Numerical Modeling of η Carinae Bipolar Outflows

R.F. González^{1,2}, E.M. de Gouveia Dal Pino², A.C. Raga¹ and P.F. Velázquez¹

ABSTRACT

In this paper, we present two-dimensional gas dynamic simulations of the formation and evolution of the η Car bipolar outflows. Adopting the interacting nonspherical winds model, we have carried out high-resolution numerical simulations, which include explicitly computed time-dependent radiative cooling, for different possible scenarios of the colliding winds. In our simulations, we consider different degrees of non-spherical symmetry for the pre-outburst wind and the great eruption of the 1840s presented by the η Car wind. From these models, we obtain important differences in the shape and kinematical properties of the Homunculus structure. In particular, we find an appropriate combination of the wind parameters (that control the degree of non-spherical symmetry) and obtain numerical experiments that best match both the observed morphology and the expansion velocity of the η Car bipolar shell. In addition, our numerical simulations show the formation of a bipolar nebula embedded within the Homunculus (the little Homunculus) developed from a secondary eruptive event suffered by the star in the 1890s, and also the development of tenuous, high velocity ejections in the equatorial region that result from the impact of the eruptive wind of the 1840s with the pre-outburst wind and that could explain some of the high speed features observed in the equatorial ejecta. The models were, however, unable to produce equatorial ejections associated to the second eruptive event.

Subject headings: ISM — hydrodynamics — shock waves — stars: individual (η Carinae) — stars: winds, outflows

¹Instituto de Ciencias Nucleares (UNAM),
Ap. Postal 70-543, CP:04510, México D.F., México
e-mail: ricardog@nuclecu.unam.mx, raga@nuclecu.unam.mx,
pablo@nuclecu.unam.mx

²Instituto Astronômico e Geofísico (USP),
R. do Matão 1226, 05508-090 São Paulo, SP, Brasil
e-mail: dalpino@astro.iag.usp.br

1. Introduction

The star η Car is one of the most luminous and massive stars of our galaxy. Its 5.5 year cyclic variability seems to indicate that it is actually a binary system (Damineli et al. 1996, 2000). Classified as a luminous blue variable star (LBV), η Car has presented eruptive events in which its wind parameters (mass loss rate and ejection velocity) were drastically increased in short periods of time (Maeder 1989, Pasquali et al. 1997). Its 20 yr great eruption (in the 1840s), in which a few solar masses ($\sim 2 M_{\odot}$) were expelled into the interstellar medium, formed two symmetrical lobes (e.g. Humphreys & Davidson 1994; Davidson & Humphreys 1997) expanding with velocities $\sim 600 \text{ km s}^{-1}$ in the polar direction (see, for instance, Smith 2002; Smith et al. 2003a). The nebular axis forms an angle of 41° with the line of sight (Davidson et al. 2001) and at a distance of $\sim 2.3\text{-}2.5 \text{ kpc}$, it has a total physical size $\sim 6 \times 10^{17} \text{ cm}$.

In the 1890s, a secondary eruptive event occurred in the η Car wind (Humphreys, Davidson, & Smith 1999). Recent spectroscopic observations have revealed the presence of a bipolar nebula embedded within the Homunculus, with an angular size of $\pm 2''$, which probably was formed from this minor eruption (e.g. Ishibashi et al. 2003) in which $\sim 0.1 M_{\odot}$ were expelled by the star. In the polar direction of the inner nebula (which also coincides with the Homunculus axis), the expansion velocity of the shell is $\sim 300 \text{ km s}^{-1}$. On the other hand, the outer Homunculus is also embedded within a low density, hot, gaseous, extended structure (called the outer ejecta), which was probably produced from previous eruptive events of the star (see, for instance, Walborn et al. 1978, Davidson & Humphreys 1997; Weis et al. 2001), or by the remnants of the blast wave of the 1843 eruption (Weis 2004).

Apart from the Homunculus, the little Homunculus, and the outer ejecta, observations of this source also reveal the presence of equatorial features that typically move with $v \sim 100 - 350 \text{ km s}^{-1}$ (e.g. Smith & Gehrz 1998; Davidson et al. 2001), although higher-speed equatorial components have been also detected with velocities $\sim 750 \text{ km s}^{-1}$ (e.g. Smith et al. 2003a) or even larger. These ejections may contain material from both the eruptions of the 1840s and 1890s (e.g. Davidson et al. 2001; Smith 2002).

Bipolar nebulae are very common phenomena in Astrophysics, surrounding not only LBVs, but also young stellar objects and low-mass stars in their late stages of evolution, like the planetary nebulae. Their formation is still a matter of debate, particularly in LBVs (e.g., Langer et al. 1994, 1999), but in general they are attributed to the collision of stellar winds emanating from the central star (e.g., Icke 1988, Frank & Mellema 1994; Frank et al. 1995, 1998; Dwarkadas & Balick 1998; Langer et al. 1999).

To produce a nonspherical bipolar nebula, most models have assumed that a spherical

fast wind expands into a nonspherical (toroidal) slow, dense wind previously ejected from the star. The high densities in the equatorial plane constrain the expansion of the fast wind in that direction and, if the density ratio between the equator and pole is high enough, the expanding spherical shell quickly becomes bipolar. The development of precursor, nonspherical *slow* winds in massive stars is naturally explained by simply invoking stellar rotation and centrifugal forces (e.g, Maeder 1989). However, *fast* winds with inherently nonspherical geometry also find theoretical support (e.g., Frank et al. 1998; Smith et al. 2003a, Smith et al. 2004, Maeder 2004). Bjorkman & Cassinelli (1992) showed that a strong equator-to-pole density contrast could form during the great eruption of η Car in the 1840s if the star was close to the Eddington luminosity limit. In this limit, the wind is deflected towards the equator close to the star because the radiative and centrifugal forces balance gravity at the equator. In a model for Be stars, Pauldrach & Puls (1990) showed that when the effective gravity of the star drops below a critical value, a discontinuity, denominated bi-stability, develops in mass and velocity. Lamers & Pauldrach (1991) have demonstrated that stellar rotation can induce latitudinal changes in the effective gravity and the optical depth of the wind that put the polar and equatorial regions on different sides of this bi-stability limit. As a consequence, a high-velocity, low-density wind should form at the poles, and a low-velocity, high-density wind should form at the equator. The LBV star AG Carinae, for example, has a wind with these characteristics. On the other hand, quite oppositely, recent numerical models of radiative line-driven winds (Owocki et al. 1996; 1998; Dwarkadas & Owocki 2002), which are based on the wind-compressed disk mechanism but include the effects on non-radial line forces, have found that the equatorial density enhancement can be inhibited and instead, an enhanced mass flux is predicted to occur toward the poles. Van Boekel et al. (2003) present VLT and VLTI observations of the present-day stellar wind of η Car that favor this model. They found evidence that the density contours in η Car’s wind are elongated along the major axis of the Homunculus. This alignment suggests that rotation may be responsible for the shape of the η Car bipolar nebula.

All the results above show that there are several ways by which fast winds may become intrinsically nonspherical from the source. In the case of the η Car wind, the observed latitudinal variations in H and HeI lines reveal that the speed, density and ionization are nonspherical near the star and indicate that its stellar wind is inherently nonspherical (Smith et al. 2003a).

Alternative models to explain the η Car nebula bipolar shape have invoked a colliding wind binary star mechanism (see, e.g., Soker 2001). However, an argument against a companion star *dominating* the wind structure is its axial symmetry. Recent STIS spectral observations in several positions along the Homunculus (Smith et al. 2003a) show the same latitudinal dependence for the velocities in both hemispheres and both sides of the polar

axis, as well as, the same P Cygni absorption in hydrogen lines on either side of the poles. Also, the high velocities seen in reflected light from the polar lobes give some evidence that the polar axis of the Homunculus is aligned with the rotation axis of the central star. This has important consequences for the formation of the bipolar lobes and the equatorial ejecta around η Car, as it may be an indication that axial symmetry and the ejection mechanism during the great eruption were directly linked to the central star’s rotation.

Frank et al. (1995) have previously developed numerical two-dimensional gasdynamical models for the origin and evolution of the η Car Homunculus. Adopting the interacting wind scenario, wherein a high-velocity isotropic stellar wind interacts with a nonspherical environment, they found that models with a strong density enhancement toward to equator (equator-to-pole density contrast ~ 200) reproduce the observed morphology and kinematics of the Homunculus. On the other hand, adopting the Bjorkman & Casinelli (1992) model described above, Langer et al. (1999) also computed two-dimensional hydrodynamic models of the interacting winds scenario including the effects of stellar rotation in order to explain the formation of the η Car Homunculus. In these models, a thick torus at the equator is required in order to reproduce the shape of the Homunculus nebula.

Recently, Frank et al. (1998) studied the opposite scenario, in which a nonspherical fast wind expands into an isotropic slower wind. They show that such nonspherical winds are able to produce bubble morphologies. However, like the previous ones, this model fails to produce the equatorial ejecta. Also, Dwarkadas & Balick (1998) have invoked the presence of a toroidal ring near the nuclear region to collimate the material expelled by the star in the great eruption of the 1840s. Though their radiative models show a fragmentation of the ring that could help to explain the observed equatorial ejecta, they only produced small velocities fragments ($\sim 40 - 100 \text{ km s}^{-1}$).

In a recent letter (González et al. 2004, hereafter Paper I), assuming that the shaping of the η Car nebula is dominated by the primary star’s winds, we have presented a hydrodynamical simulation involving the interaction of intrinsically nonspherical winds. Adopting an appropriate combination of the parameters that control the degree of non-spherical symmetry of the winds, we have found that the impact between the major eruption and the lighter pre-outburst flow can result in the formation of the bipolar nebulae and high-velocity equatorial ejections which are observed around η Car. In order to obtain from numerical simulations the set of parameters that best match the observations of the η Car nebula, in the present paper we present a comparison between several possible scenarios of the colliding wind model in which we have considered different combinations of the non-spherical symmetry parameters of the interacting winds.

The paper is organized as follows. In §2, we describe the model. In §3, we present the

numerical simulations with a discussion of the results. Finally, we give our conclusions in §4.

2. The Model

As in Paper I, the generalized nonspherical interacting stellar winds scenario is adopted. We first assume that before the great eruption in 1840, η Car deposited many solar masses into the interstellar medium, creating a toroidal environment (the pre-outburst wind) in which the density and the velocity are characterized by (see Frank et al. 1995, 1998),

$$n = n_0 \left(\frac{r_0}{r} \right)^2 \frac{1}{F_\theta}, \quad (1)$$

$$v = v_0 F_\theta, \quad (2)$$

respectively, where r_0 is the injection radius (assumed to be of a few stellar radii), and

$$F_\theta = 1 - \alpha [(1 - e^{-2\beta \sin^2 \theta}) / (1 - e^{-2\beta})] \quad (3)$$

which controls the variation of the flow parameters from the equator ($\theta = 90^\circ$) to the polar direction (at $\theta = 0$). The parameter α is related to the equator-to-pole density contrast $n_e/n_p = 1/(1-\alpha)$, and β controls the shape of the wind. Equations (1) and (2) imply the simple case of constant mass loss rate ($\dot{M} \propto n v$) as a function of polar angle. The great eruption and most of the wind phases that follow this outburst are also assumed to be nonspherical with their initial shapes also modulated by equations (1)-(3).

In order to perform numerical simulations of the η Car winds, the *non-spherical* parameters of the model (α and β) must be specified for the different wind phases. It is possible to estimate these constants simply matching the models to the observed morphology of the Homunculus structure around η Car. Assuming spherical symmetry for the great eruption, Frank et al. (1995) found that models with $\alpha > 0.99$ and $1 < \beta < 2.5$ for the pre-outburst wind produce morphologies that best match the observations.

Another possibility for fixing the non-spherical parameters α and β is to use the kinematical properties of the Homunculus. Smith (2002) measured the expansion velocity (in H_2) of the polar lobes and calculated the physical size of the nebula at different latitudes, adopting a distance of 2250 pc and an age of 158 yr. In Figure 1, we have fitted Smith's observations with eq. (2) and obtained much smaller values for the parameters above ($\alpha \simeq 0.78$

and $\beta \simeq 0.3$). In the present analysis, we have examined different combinations of this pair of parameters for the interacting winds along the evolution history of η -Car outflow (see below).

3. Numerical Simulations

Considering the high degree of axial symmetry of the η -Car nebulae, we have carried out two-dimensional (instead of three-dimensional) gasdynamic numerical simulations of the η Car wind using the adaptative grid Yguazú-a code. In this code (originally developed by Raga et al. 2000; see also Raga et al. 2002), the hydrodynamic equations are explicitly integrated with a set of continuity equations for the atomic/ionic species H I, H II, He I, He II, He III, C II, C III, C IV, O I, O II, and O III. The flux-vector splitting algorithm of Van Leer (1982) is employed. The simulations were computed on a four-level binary adaptative grid with a maximum resolution of 7.81×10^{14} cm, corresponding to 512×512 grid points extending over a computational domain of $(4 \times 10^{17}) \times (4 \times 10^{17})$ cm.

For the different elements that have been used for the simulations, we have used the abundances (H, He, C, O) = (0.9, 0.099, 0.07, 0.03), by number. Different C and O abundances will affect the cooling function, so that for lower C and O abundances larger post-shock cooling distances would be obtained in the numerical simulations.

3.1. Initial Physical Conditions

Table 1 lists the different possible scenarios that we have studied in this paper. Different values of the parameters α and β (that control the degree of asymmetry of the interacting winds) have been tried. In runs A-E, we have carried out numerical simulations only of the the great eruption suffered by η Car in the 1840s. In runs F-G we have also considered the minor eruption that blew out from η Car fifty years later, in the 1890s, from which it is believed that the internal Homunculus was formed (e.g. Ishibashi et al. 2003).

In all runs, we have assumed that the computational domain is initially filled by a homogeneous ambient medium with temperature $T_a = 100$ K and density $n_a = 10^{-3}$ cm $^{-3}$. A pre-outburst wind was then injected into this unperturbed environment. For this wind, in runs A-D and F-G we have adopted a terminal velocity (in the polar direction) $v_0 = 250$ km s $^{-1}$, and a mass loss rate $\dot{M} = 10^{-3}$ M $_{\odot}$ yr $^{-1}$ (e.g. Humphreys & Davidson 1994; Davidson & Humphreys 1997; Hillier et al. 2001; Corcoran 2001), which is injected at a distance $r_0 = 1 \times 10^{16}$ cm from the stellar surface with a temperature $T_0 = 10^4$ K. When the

slow wind reaches the edge of the computational domain along the symmetry axis (y -axis) forming a toroidal environment, a much faster and massive wind is turned on for 20 years (this is the estimated duration of the great eruption; see Davidson & Humphreys 1997). It is expelled from the star with a velocity of 715 km s^{-1} , mass loss rate of $7 \times 10^{-2} M_{\odot} \text{ yr}^{-1}$, and temperature of 10^4 K . After this major eruption, a third outflow (the post-outburst wind) with similar conditions as the pre-outburst wind resumes. Additionally, in runs F-G we consider another eruptive event which occurs fifty years after the great eruption. For 10 years, the wind parameters are increased to 317 km s^{-1} and $10^{-2} M_{\odot} \text{ yr}^{-1}$, after which the original slow wind again resumes until the present days. In run E we have assumed a faster pre-outburst wind with $v_0 = 500 \text{ km s}^{-1}$ (in the polar direction) and $\dot{M} = 10^{-3} M_{\odot} \text{ yr}^{-1}$. In this case, during the great eruption, the wind parameters taken to be $v_0 = 655 \text{ km s}^{-1}$ and $7 \times 10^{-2} M_{\odot} \text{ yr}^{-1}$.

3.2. Results from the Simulations

In this section, we present the temperature, density, pressure and velocity maps computed for the different scenarios considered in this paper. Important differences in the shape and kinematics of the Homunculus (and, also, of the inner nebula formed from the minor eruption) have been found between the models. As in previous numerical simulations (e.g. Frank et al. 1995, 1998), all runs show that the momentum flux is mainly dominated by the great and minor eruptions, so that the post-outburst slow winds have no significant effect on the kinematics of the shell structures, which (at high latitudes) expand almost ballistically.

In run A, we have considered the simple case of an isotropic, eruptive wind ($\alpha_2 = 0$) colliding with a pre-outburst, nonspherical outflow with the non-spherical symmetry parameters estimated from Smith’s observations (2002) of the expansion velocity of the Homunculus ($\alpha_1 = 0.78$ and $\beta_1 = 0.3$; see Fig. 1). In Figure 2, we present the stratifications of the temperature (top left), density (top right), pressure (bottom left), and velocity (bottom right) computed from run A at a time 160 yr after the great eruption. At this time, the fast wind has filled almost completely the computation domain. Near the polar direction (at high latitudes), a double-shock structure is seen, with an outward shock accelerating the pre-eruptive wind and an inward shock decelerating the material expelled in the great eruption. The expansion velocity of the shocks (at the poles) has an intermediate velocity between the pre-outburst wind and the great eruption ($\sim v_c \simeq 635 \text{ km s}^{-1}$; see Cantó et al. 2000; González & Cantó 2002), and decreases for smaller latitudes (see eq. [2]). We note that the expansion of the spherical fast wind into the pre-outburst wind has practically destroyed the toroidal shape of the later. From this interaction, a relatively hot ($T \sim 10^3 \text{ K}$) and faint

TABLE 1

ASYMMETRY PARAMETERS
OF THE COLLIDING WINDS

Run	<i>Pre-outburst</i> ⁽¹⁾		<i>Great Eruption</i> ⁽²⁾		<i>Minor Eruption</i> ⁽³⁾	
	α_1	β_1	α_2	β_2	α_3	β_3
A	0.78	0.30	0.00	–	–	–
B	0.78	0.30	0.78	0.30	–	–
C	0.90	1.50	0.78	0.30	–	–
D ⁽⁴⁾	0.90	1.50	0.78	0.30	–	–
E ⁽⁵⁾	0.90	1.50	0.78	0.30	–	–
F	0.90	1.50	0.78	0.30	0.00	–
G	0.90	1.50	0.78	0.30	0.78	0.30

(1) $v_0 = 250 \text{ km s}^{-1}$ (runs [A-D; F-G]); $\dot{M} = 10^{-3} \text{ M}_\odot \text{ yr}^{-1}$

(2) $v_0 = 715 \text{ km s}^{-1}$ (runs [A-D; F-G]); $\dot{M} = 7 \times 10^{-2} \text{ M}_\odot \text{ yr}^{-1}$

(3) $v_0 = 317 \text{ km s}^{-1}$; $\dot{M} = 10^{-2} \text{ M}_\odot \text{ yr}^{-1}$

(4) In this run, $n \propto F_\theta$ in the pre-outburst wind (see eq. [1])

(5) In this run, $v_0 = 500 \text{ km s}^{-1}$ in the pre-outburst wind
and 655 km s^{-1} in the great eruption

($\rho \simeq 10^{-22}$ g cm $^{-3}$) bubble is produced, which expands toward high latitudes. The inner emerging bipolar structure seen near the center of the system is the post-outburst wind that has arisen with the same initial conditions of pre-outburst wind.

In run B, we have considered the interaction of an eruptive wind with a pre-outburst wind both nonspherical and with the same non-spherical symmetry parameters ($\alpha = 0.78$ and $\beta = 0.3$, see Table 1). Figure 3 shows the results for this scenario at a time $t = 160$ yr after the great eruption turn-on. The numerical simulation shows the formation of a bipolar structure with a latitude-dependent expansion velocity that is very similar to the actual η Car Homunculus (see Smith 2002), though, as mentioned in Paper I, the length to width ratio of the Homunculus is somewhat larger than in the images of η Car (this difference could be partially attributed to projection effects that have not been considered in this work). At the time depicted, almost all of the fast material has gone through the inner shock, producing a rarefied region with a mean temperature $T \simeq 10^2$ K and density $\rho \simeq 10^{-23}$ g cm $^{-3}$ inside the bubble. As in run A, this model does not produce any ejections in the equatorial direction.

The numerical results obtained from runs A and B, suggest that an appropriate combination of the parameters that control the degree of non-spherical symmetry of the interacting winds could reproduce both the bipolar shell with the latitude-dependent expansion velocity of the Homunculus and some equatorial ejection as observed in this source.

In run C we have computed another possible colliding wind scenario, in which the non-spherical symmetry parameters for the eruptive and pre-outburst winds were assumed to be different. For the great eruption, we have adopted the parameters estimated from the expansion velocity of the Homunculus ($\alpha = 0.78$ and $\beta = 0.3$; see Fig. 1), and for the pre-outburst wind we have increased them (to 0.9 and 1.5, respectively) in order to obtain a larger equator-to-pole density contrast (see §2) with a less confined density distribution in the equatorial plane (see Frank et al. 1995).

In Figure 4, we present the results computed from run C. Under the conditions above, the impact of the two wind shock fronts (initially at the equator) occurs at a distance ~ 3300 AU at $t \sim 100$ yr from the great eruption. The temperature and density maps show the formation of a hot, tenuous structure ($T \simeq 10^7$ K, $\rho \simeq 5 \times 10^{-19}$ g cm $^{-3}$) at low latitudes that is absent in the previous models. This feature reaches a maximum expansion velocity of ~ 700 km s $^{-1}$ (see the velocity map of Fig. 4) and could be related to the outer high-velocity parts of the observed equatorial ejecta in η Car. The observations of Smith et al. (2003a) of material confined to the equatorial plane (northeast of the central star) indicate an expansion velocity of 750 km s $^{-1}$, which is in quantitative agreement with our numerical results.

Recent observations of P Cygni absorption line profiles (in hydrogen lines) at different latitudes of the η Car Homunculus give evidence that the density (and ionization) structure in scales of ~ 100 AU of the current η Car wind is nonspherical (see Smith et al. 2003a), and the deeper absorption at high latitudes suggests an increase in both the velocity and the density toward the polar direction. In run D, we have assumed that these conditions were already present in the η Car wind before the great eruption adopting $v \propto F_\theta$ and $n \propto F_\theta$ (see eqs. [1-3] in §2). In this way, we have forced the nonspherical outburst wind of the 1840s to impinge into a slow pre-outburst wind with a larger density (and larger mass-loss rate) towards the polar direction. We find that this scenario is unable to develop significant narrow equatorial ejection (see Fig. 5).

From the different scenarios described above (runs A-D) and presented in Figures 2-5, we observe that the interaction of the colliding winds near the polar direction is very similar in all models. At $\theta \simeq 0$ (high latitudes), the function that describes the non-spherical symmetry of the winds has a value $F_\theta \simeq 1$ (see §2) and, therefore, all the models have approximately the same behavior at the poles.

As noted before, we find from the simulations that a double-shock structure develops in the Homunculus, with an outward shock that sweeps up the material of the precursor wind and an inward shock that decelerates the outburst wind material coming from behind. The compression (followed by radiative cooling) of the shocked material behind both shocks develops relatively thin, cold shells (see the density and pressure maps). These results are consistent with thermal-IR observations (e.g., Smith et al. 2003b), and observed shocked molecular hydrogen and [FeII] emission (Smith 2002, 2004) that indicate the existence of a double shell structure in the polar lobes.

Using the one-dimensional radiative shock models developed by Hartigan et al. (1987), we estimated the cooling time and distance of both shocks (see also Paper I). For high-velocity shocks ($v_s > 80$ km s⁻¹), the radiative cooling time is given by $t_c \simeq 320 \text{ yr } v_{s,100}^{1.12} \rho_{pre,-22}^{-1}$, where $v_{s,100}$ is the shock speed in units of 100 km s⁻¹, and $\rho_{pre,-22}$ is the preshock density in units of 10^{-22} g cm⁻³. In the polar direction, the inward shock speed $v_s \simeq 80$ km s⁻¹ and the pre-shock density $\rho_{pre} \simeq 5.1 \times 10^{-20}$ g cm⁻³ give a $t_c \simeq 0.5$ yr cooling time, which is very short compared with the estimated age of the η Car Homunculus (~ 160 yr). As a consequence, the estimated cooling distance, $d_c \simeq 3.7 \times 10^{14}$ cm $v_{s,100}^{4.73} \rho_{pre,-22}^{-1} = 2.5 \times 10^{11}$ cm is very small compared with the physical size of the nebula ($\sim 3.2 \times 10^{17}$ cm; e.g. Smith 2002). This value qualitatively explains the narrowness of the cold inner shell seen in our simulations, which has a temperature $\sim 10^4$ K and a density $\sim 3 \times 10^{-19}$ g cm⁻³. On the other hand, at the outward shock, the higher polar shock velocity $v_s \simeq 400$ km s⁻¹ and the smaller preshock density $\rho_{pre} \simeq 2.1 \times 10^{-21}$ g cm⁻³ give a much larger cooling time $t_c \simeq 69$

yr and cooling distance $d_c \simeq 1.6 \times 10^{16}$ cm, explaining the thick polar cap seen behind the outer shock in our numerical experiments (with a thickness $\sim 3 \times 10^{16}$ cm, a temperature $\simeq 2 \times 10^4$ K, and a density $\rho \simeq 5 \times 10^{-21}$ g cm $^{-3}$). This cooling distance is also comparable to the thickness of the observed polar cap of the Homunculus in the η Car wind ($\sim 1'' = 2500$ AU; e.g. Smith et al. 2003a, Smith 2004).¹

Currie et al. (2002) discovered a high velocity shell surrounding the southeast lobe of the Homunculus which expands faster than its front wall. The emission lines detected in this feature suggests that a much faster stellar wind might have been present before the great eruption of the 1840s. In run E, we investigate this possibility and study its implications on the morphology and kinematics of the η Car Homunculus.

The toroidal pre-outburst wind is created from the interaction between a high velocity stellar wind (expanding with a $v_0 = 500$ km s $^{-1}$ velocity in the polar direction) and the homogeneous environment. Matching Smith’s observations (2002) of the expansion velocity of the Homunculus, we then obtain a velocity of 655 km s $^{-1}$ for the great eruption. In this case, the parameters that control the degree of non-spherical symmetry of the interacting winds are the same as in run C. The mass loss rate of the pre-outburst wind and the great eruption are $\dot{M} = 10^{-3} M_\odot$ yr $^{-1}$ and $7 \times 10^{-2} M_\odot$ yr $^{-1}$, respectively.

In Figure 6, we present the results for this run ~ 160 yr after the great eruption. We observe that this model produces a morphology and kinematics similar to the η Car lobes, but with much less dense ($\rho \simeq 10^{-21}$ g cm $^{-3}$) and slower equatorial skirt (~ 200 km s $^{-1}$) than that of run C (see Fig. 4).

Numerical simulations of run C including also the second eruptive event of η Car in the 1890s, are presented in Figures 7 and 8 (corresponding to the runs F and G, respectively). In both models, the second eruptive wind was injected 50 years after the great eruption, following a more quiescent wind phase (i.e., the post-outburst wind after the great eruption). In the two figures, we observe the formation of a bipolar nebula embedded within the Homunculus.

The existence of such a structure was deduced from the observations of Ishibashi et al. (2003). The spherical symmetry assumed for this minor eruptive wind in run F (Fig. 7) produces a little Homunculus expanding in the polar direction with velocity $v = 300$ km s $^{-1}$. At the equator, the interaction of the shock fronts of the inner and outer Homunculus starts at 110 yr after the minor eruption and we find that there is almost no contribution to the outer

¹We note that although the present simulations do not include radiative cooling due to molecules and the gas behind the shocks cannot cool to temperatures as low as \sim few 100 K, the densities obtained from the simulations are not far from those obtained for the gas from IR observations of the dusty Homunculus shell ($\sim 10^{-20}$ g cm $^{-3}$, Smith 2004).

equatorial ejecta from the material expelled in the minor eruption, Its material is mainly inside the walls of the bubble of the outer Homunculus. Therefore, in our simulations the outer, high speed equatorial ejecta are produced only by the interaction of the great eruption (of the 1840s) with the pre-outburst wind.

In run G (Fig. 8), motivated by recent UV images within 0.2 arcsec of the star (that have revealed the existence of a little internal torus which could be related to the little Homunculus and could signify that a recurrent mass ejection with the same geometry as that of the great eruption might have occurred; Smith et al. 2003c), we have assumed the same non-spherical symmetry parameters for the minor eruption as those of the great eruption wind (see Table 1). In this case, the resulting inner Homunculus nebula follows the shape of the outer one, but it also fails to produce equatorial ejections and the shock fronts of the two Homunculi do not even interact during their lifetime.

In the polar direction, both numerical simulations show a thickness of $\sim 10^{16}$ cm for the expanding shell of the inner Homunculus.

In Figure 9, we present the logarithmic-scale density maps in four quadrants of model F for four different times ($t = 10, 60, 110$ and 160 yr) of evolution since the great eruption (taken from Paper I). We observe more clearly from these simulations of the evolution (of the five interacting winds) the formation of the bipolar nebulae with shapes similar to the large and little Homunculi of η Car. The impact of the large Homunculus with the shock front of the pre-outburst wind (which occurs ~ 100 yr after the great eruption) causes the formation of the low density equatorial ejection mentioned above (see the bottom-right panel of Fig. 9, and also Fig. 2 of Paper I).

4. Discussion and Conclusions

Adopting the interacting stellar wind scenario, we have carried out numerical simulations of the formation and evolution of the η Car bipolar outflows. Different possible scenarios have been investigated, which consider several combinations of the parameters that control the degree of non-spherical symmetry of the colliding winds. Our models show important differences in the shape and kinematics of the Homunculus and the little Homunculus, but suggest that the formation of the bipolar nebulae and the high-velocity features observed in this source can result from the impact of intrinsically nonspherical winds coming from the central star.

In a first attempt, we have tried to simulate, as in previous work (Frank et al. 1995; Langer et al. 1999; Dwarkadas & Balick 1998, the η Car nebulae assuming a fast, spherical

eruptive wind impinging on a dense, slow toroidal pre-outburst wind. For the later, we have assumed nonspherical density and velocity distributions estimated from the observations of Smith (2002) of the expansion velocity of the Homunculus structure at different latitudes. Given the small equator-to-pole density contrast (~ 4.5) of the pre-outburst wind in this case, the numerical experiment has shown that the fast flow of the great eruption quickly sweeps the toroidal pre-outburst almost eliminating the (non-spherical) bipolar shape (Fig. 1, run A).

We then considered the interaction of intrinsically nonspherical winds. Adopting the same angular distribution (in density and velocity) for the great eruption and the pre-outburst wind estimated from the observations of Smith (2002), our numerical simulations have shown that a bipolar shell with the shape and kinematics of the observed Homunculus nebula around η Car naturally develops (Fig. 3, run B). However, this model is not able to produce (at least not within a ~ 160 yr period of evolution since the major eruption) high-velocity features near the equatorial plane, as those observed in the HST images of this source (e.g. Morse et al. 1998, Smith et al. 2003a).

In order to obtain the formation of both the outer Homunculus structure and the equatorial ejecta, we have simulated the interaction of nonspherical winds (the great eruption and the pre-outburst wind) with different degrees of non-spherical symmetry. We have found an appropriate combination of the non-spherical symmetry parameters that best match the observations of η Car (see Figs. 4 and 9). The numerical simulations of this model (run C) show the formation of a tenuous and narrow, high-velocity equatorial ejection (with a maximum expansion velocity of ~ 700 km s $^{-1}$) arising from the impact of the Homunculus with the shock front of the pre-eruptive torus at the equator. This equatorial ejection could correspond to the high velocity components of the equatorial skirt observed in the η Car nebula (also, see Paper I).

Based on data from the current η Car wind observed within scales of ~ 100 AU (Smith et al. 2003a), we have also carried out numerical simulations assuming similar conditions for the past winds, i.e., a larger density, velocity and mass loss rate in the polar direction than in the equator for the pre-outburst wind that preceded the great eruption. In this model (run D), a structure that resembles the Homunculus is indeed formed, but the very faint equatorial features suggest that the conditions of the η Car wind before the great eruption were probably not the same as the current ones.

Additionally, we have also investigated a possible scenario (run E) with a higher velocity pre-outburst wind, as suggested from the observations of Currie et al. (2002). We found that a bipolar nebula with morphology and kinematics similar to the η Car Homunculus is formed, but the numerical simulations obtained from this model show a very rarefied

equatorial ejection (Fig. 6). This result indicates that the high-velocity shell observed by Currie et al. (2002) does not necessarily imply a relatively high-velocity pre-outburst wind just before the great eruption. The high-velocity features observed at high latitudes outside the Homunculus nebulae of η -Car, and the observed outer ejecta in general (Weis et al. 2001, Weis 2004), could perhaps be the relics of a previous eruptive event (possibly with similar strength to the great eruption). The presence of eruptions and sudden variability in the light curve of η -Car every 50 years since the great eruption (Humphreys 2004) is an indication that similar events could have occurred also in the past, before the great eruption (de Gouveia Dal Pino et al. 2004).

The numerical experiments (Figs. 7 and 8) including the second eruptive event (which we have called the minor eruption) of η Car fifty years after the great eruption show the formation of an internal bubble with a bipolar shape very similar to the one implied by the observations of the little Homunculus of Ishibashi et al. (2003). In particular, run G (Fig. 7) in which the minor eruption has been simulated with the same geometry as the great one, produces a little Homunculus with the same shape as the outer Homunculus. However, little can be said in favor of one model over the other one (runs F and G) as detailed observations of the geometry and kinematics of the little Homunculus are still required.

In spite of recent spectroscopic observations that provide evidence of equatorial gas with low and high velocities, probably associated with both the 1840s and the 1890s eruptions (e.g. Davidson et al. 2001), in our simulations there is almost no contribution of the minor eruption to the high speed equatorial ejecta. This suggests that some extra physical ingredient may be missing in our numerical model. A potential mechanism could be rotation. If rotation was present, the associated centrifugal forces could help to push part of the inner eruptive wind outwards through the walls of the homunculus nebulae in the equatorial region thus producing a slow ejection component in that direction.

Finally, we mention the new work of Matt & Balick (2004), who have modelled the Homunculus in terms of a steady, MHD wind from a rotating source with a dipole magnetic field (which is aligned with the rotation axis). In the future, models incorporating both the time-dependence of the successive eruptions (as in our present paper) and the effects of the stellar rotation and magnetic field (as in the work of Matt & Balick 2004) should be studied. Another new observational result is that the mass of the Homunculus could be much larger (Smith et al. 2003b). Models incorporating this result should also be attempted in the future.

E.M.G.D.P. has been partially supported by grants of the Brazilian Agencies FAPESP and CNPq. R.F.G., A.C.R. and P.F.V. acknowledges CONACyT grants 36572-E and 41320

and the DGAPA (UNAM) grant IN112602. The authors have benefited from elucidating conversations and comments from Augusto Damineli, Nathan Smith, Kazunori Ishibashi, and Kris Davidson. The authors also thank the useful comments of an anonymous referee.

REFERENCES

- Bjorkman, J.E., & Cassinelli, J.P. 1992, ASP Conference Series, Vol. 22, 88
- Cantó, J., Raga, A.C., & D'Alessio, P. 2000, MNRAS, 313, 656
- Corcoran, M.F., Ishibashi, K., Swank, J.H., & Petre, R. 2001, ApJ, 547, 1034
- Currie, D.G., Dorland, B.N., & Kaufer, A. 2002, A&A, 389, L65
- Damineli, A. 1996, ApJ, 460, L49
- Damineli, A. et al. 2000, ApJ, 528, L101
- Davidson, K., & Humphreys, R.M. 1997, ARA&A, 35, 1
- Davidson, K., Smith, N., Gull, T.R, Ishibashi, K., & Hillier, D.J. 2001, AJ, 121, 1569
- Dwarkadas, V.V., & Balick, B. 1998, AJ, 116, 829
- Dwarkadas, V.V., & Owocki, S.P. 2002, ApJ, 581, 1337
- de Gouveia Dal Pino, E.M., Gonzalez, R.F., Raga, A.C., & Velazquez, P.F. 2004, in ASP Conf. Ser., The Fate of Most Massive Stars, eds. K. Davidson & R. Humphreys (San Francisco: ASP), in press
- Frank, A., Balick, B., & Davidson, K. 1995, ApJ, 441, L77
- Frank, A., & Mellema, G. 1994, A&A, 289, 937
- Frank, A., Ryu, D., Davidson, K. 1998, ApJ, 500, 291
- González, R.F. 2002, Ph. D. thesis, Univ. Nac. Autónoma México
- González, R.F., & Cantó, J. 2002, ApJ, 580, 459
- González, R.F., de Gouveia Dal Pino, E.M., Raga, A.C., & Velázquez, P.F. 2004, ApJ, 600, L59 (Paper I)
- Hartigan, P., Raymond, J., & Hartmann, L. 1987, ApJ, 316, 323
- Hillier, D.J., Davidson, K., Ishibashi, K., & Gull, T. 2001, ApJ, 553, 837

- Humphreys, R. 2004, in ASP Conf. Ser., The Fate of Most Massive Stars, eds. K. Davidson & R. Humphreys (San Francisco: ASP), in press
- Humphreys, R.M., & Davidson, K. 1994, PASP, 106, 1025
- Humphreys, R.M., Davidson, K., & Smith, N. 1999, PASP, 111, 1124
- Icke, V. 1988, A&A, 202, 177
- Ishibashi, K., et al. 2003, AJ, 125, 3222
- Lamers, H.J.G.L.M., & Pauldrach, A.W.A. 1991, A&A, 244, L5
- Langer, N., García-Segura, G., & Mac Low, M. 1999, ApJ, 520, L49
- Langer, N., Hamann, W.-R., Lennon, M., Najarro, F., Pauldrach, A.W.A., & Puls, J. 1994, A&A, 290, 819
- Maeder, A. 1989, in The Physics of Luminous Blue Variables, ed. K. Davidson, A.F.J. Moffat, & H.J.G.L.M. Lamers (Dordrecht:Kluwer), 15
- Maeder, A. 2004, in ASP Conf. Ser., The Fate of Most Massive Stars, eds. K. Davidson & R. Humphreys (San Francisco: ASP), in press
- Matt, S., & Balick, B. 2004, ApJpreprint doi:10.1086/424727
- Morse, J.A., Davidson, K., Bally, J. Ebbets, D., Balick, B. & Frank, A. 1998, AJ, 116, 2443
- Owocki, S.P., Cranmer, S.R., & Gayley, K.G. 1996, ApJ, 472, L115
- Owocki, S.P., Gayley, K.G., & Cranmer, S.R. 1998, in ASP Conf. Ser. 131, Boulder Munich II: Properties of Hot Luminous Stars, ed. I.D. Howarth (San Francisco: ASP), 237
- Pasquali, A., Langer, N., Schmutz, W., Leitherer, C., Nota, A., Hubeny, I., & Moffat, A.F.J. 1997, ApJ, 478, 340
- Pauldrach, A.W.A., & Puls, J. 1990, A&A, 237, 409
- Raga, A.C., de Gouveia Dal Pino, E.M., Noriega-Crespo, A., Mininni, P.D., & Velázquez, P.F. 2002, A&A, 392, 267
- Raga, A.C, Navarro-González, R., & Vilagrán-Muniz, M. 2000, Rev. Mex. Astron. Astrof., 36, 67
- Smith, N. 2002, MNRAS, 337,1252
- Smith, N. 2004, in ASP Conf. Ser., The Fate of Most Massive Stars, eds. K. Davidson & R. Humphreys (San Francisco: ASP), in press

- Smith, N., Davidson, K., Gull, T.R., Ishibashi, K., & Hillier, D.J. 2003a, ApJ, 586,432
- Smith et al. 2003b, AJ, 125, 1458
- Smith, N., et al. 2003c, ApJ, (in press)
- Smith, N., et al. 2004, ApJ, 605, 405
- Smith, N., & Gehrz, R.D. 1998, AJ, 116, 823
- Van Boekel, R. et al. 2003, A&A, 410, L37
- Walborn, 1978, ApJ, 219, 498
- Weis, K. 2004, in ASP Conf. Ser., The Fate of Most Massive Stars, eds. K. Davidson & R. Humphreys (San Francisco: ASP), in press
- Weis, K., Duschl, W.J., & Bomans, D.J. 2001, A&A, 367, 566

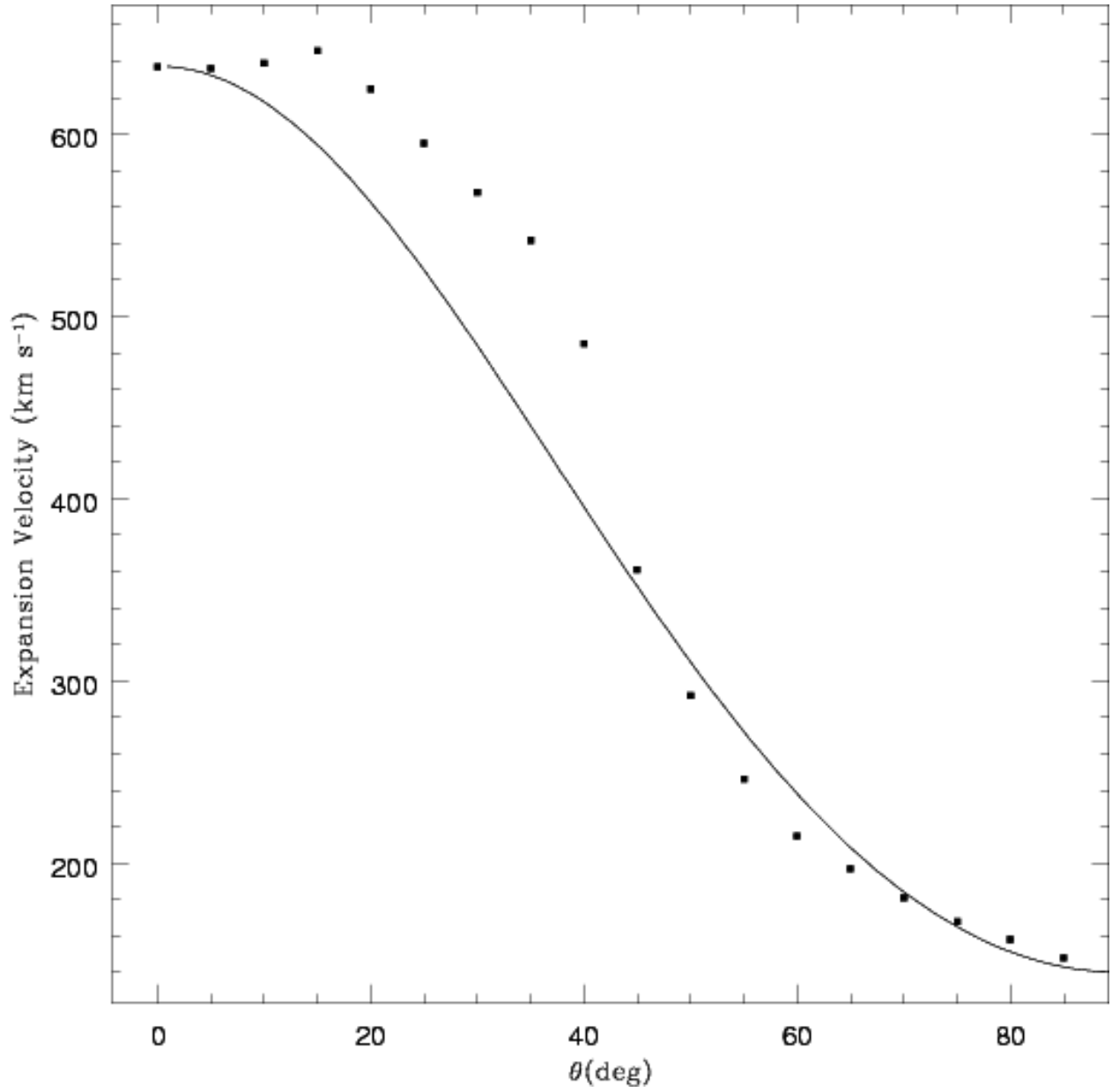


Fig. 1.— Predicted expansion velocity of the polar lobes (solid line) with $\alpha= 0.78$ and $\beta= 0.3$ (see eqs. [2]-[3]), and the observed velocity in H_2 (taken from Smith 2002) at different latitudes of the η Car Homunculus (with $\theta = 0$ at the pole).

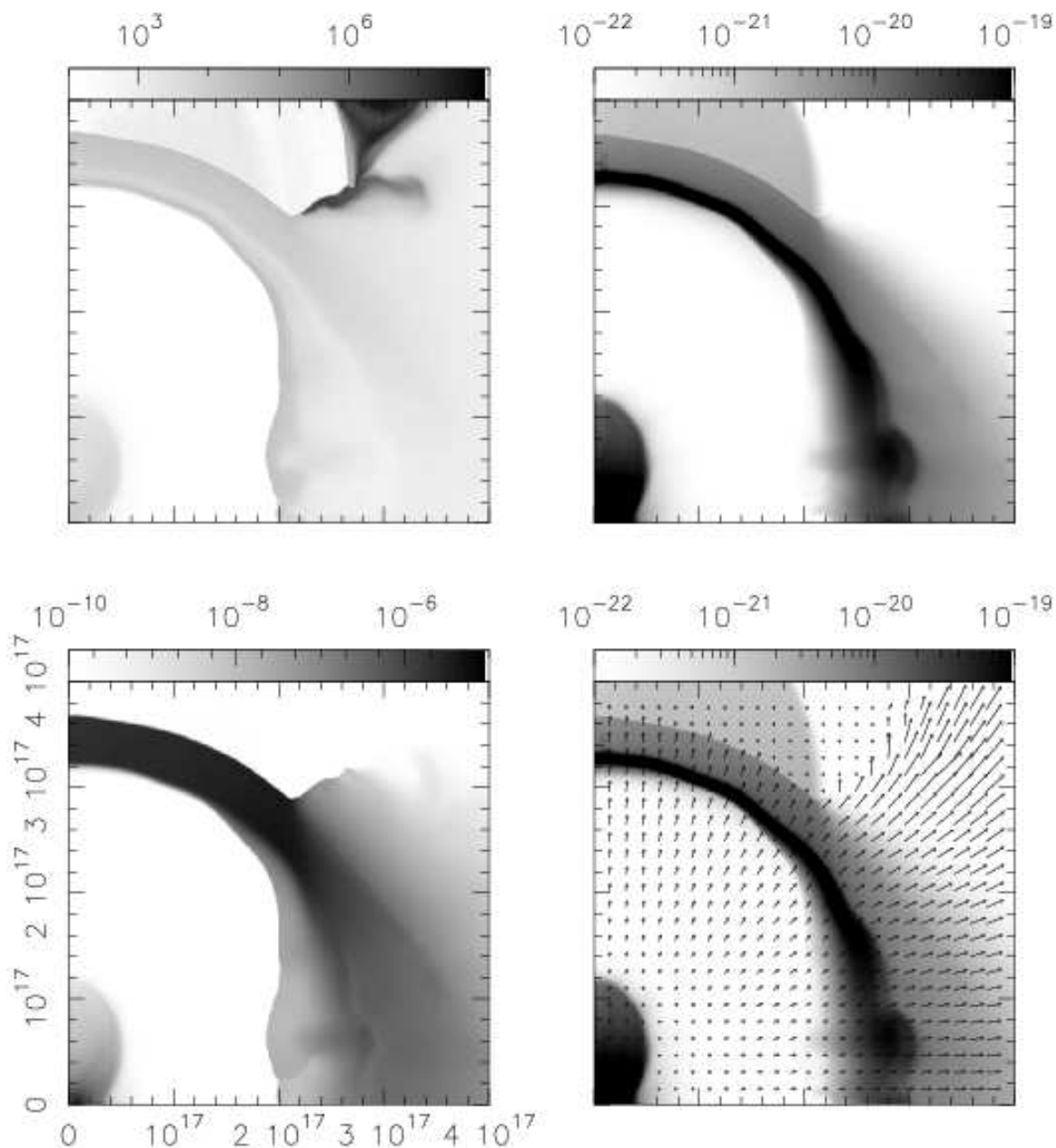


Fig. 2.— Temperature, density, pressure and velocity-field maps (top left, top right, bottom left and bottom right, respectively) for run A (which assumes that an isotropic outflow impacts into a nonspherical pre-outburst wind; see Table 1), at $t = 160$ yr of evolution after the great eruption. The units of the scales in the bars are K (for the temperature, top left), dyn cm^{-2} (for the pressure, bottom left), and g cm^{-3} (for the density, top and bottom right). The velocity map is an overlay of the density stratification (in grey scale) and the velocity-field (in arrows) corresponds to velocities between $\sim 100 \text{ km s}^{-1}$ and $\sim 1200 \text{ km s}^{-1}$. It can be observed that the expansion of the fast wind tends to make the outflow shape almost spherical. The axial (vertical) and radial (horizontal) coordinates are labeled in cm.

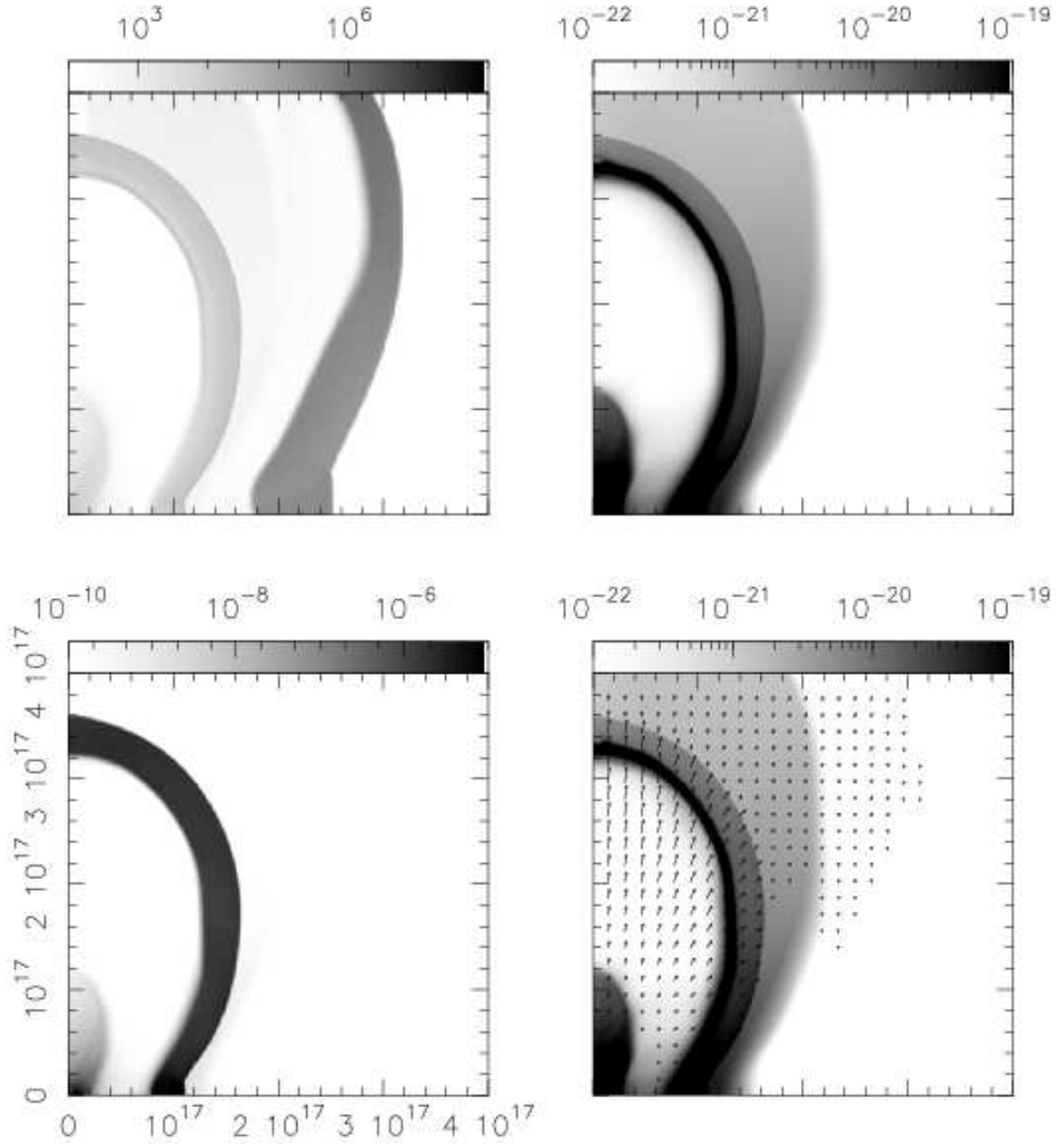


Fig. 3.— The same as Fig. 2, but for run B (which assumes the interaction of nonspherical winds with the same degree of asymmetry; see Table 1). The temperature (top left), density (top right), pressure (bottom left) and velocity-field (bottom right) maps (at $t = 160$ yr after the great eruption) computed from run B are presented. The formation of a bipolar structure like the Homunculus around η Car is seen. However, an equatorial ejecta is not produced in this scenario.

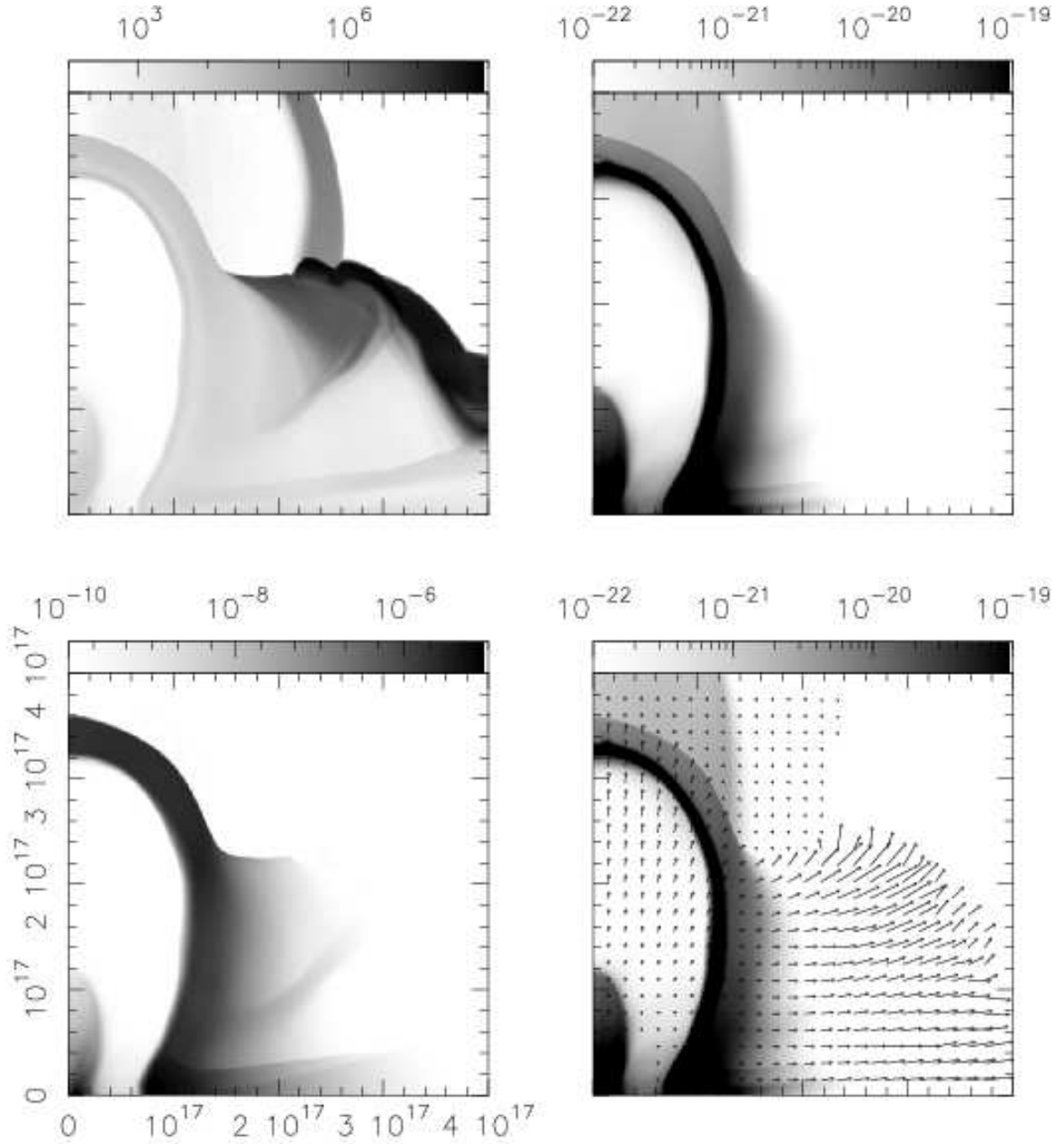


Fig. 4.— The same as Fig. 2, but for run C (which assumes the interaction of nonspherical winds with different degree of asymmetry; see Table 1). The stratifications of the temperature (top left), density (top right), pressure (bottom left) and velocity-field (bottom right) obtained for run C at $t = 160$ yr since the major eruption are presented. It can be observed that the impact of the Homunculus with the pre-outburst shock front results in the formation of hot features ($T \approx 10^7$ K) near the equatorial plane.

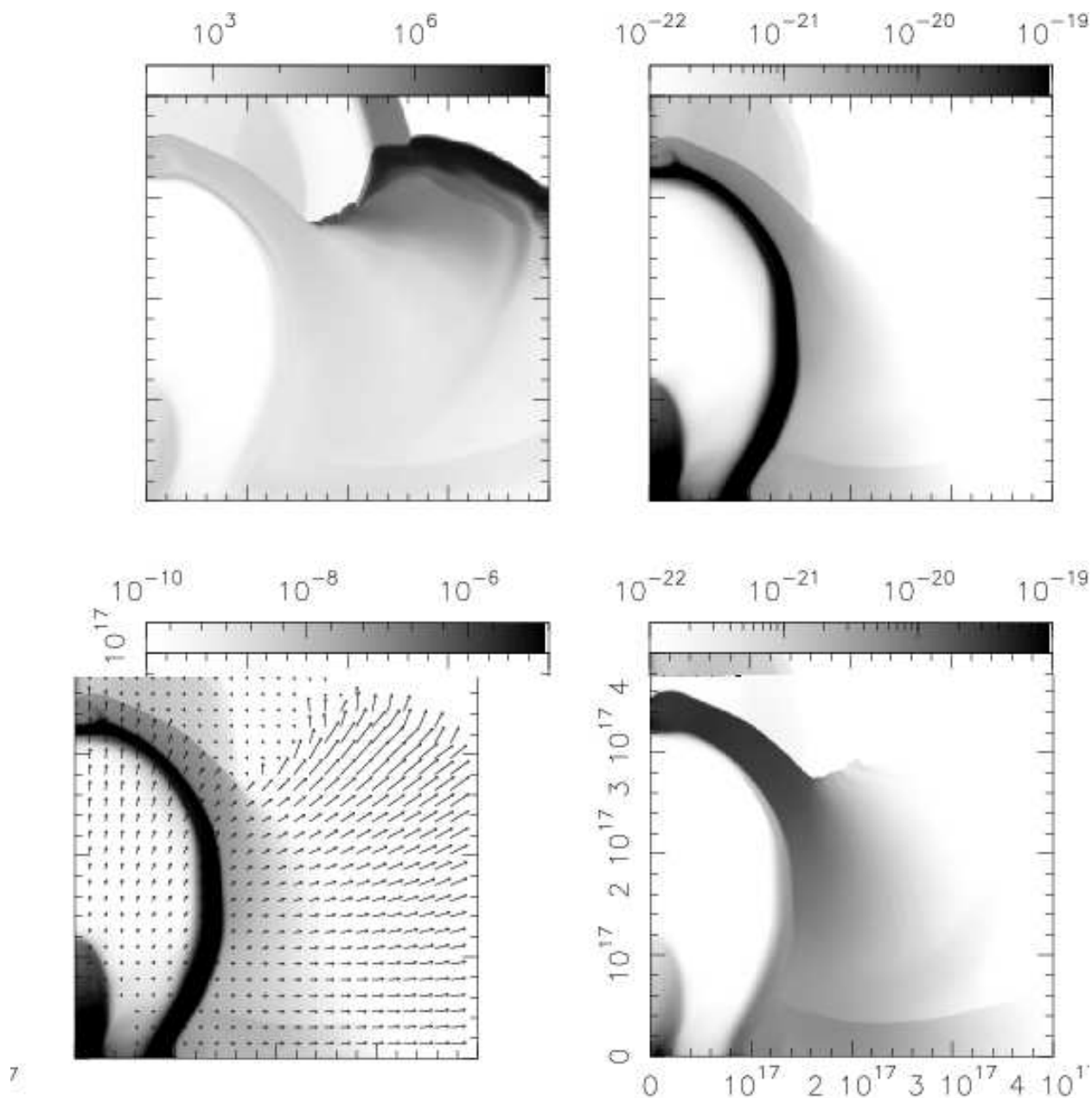


Fig. 5.— The same as Fig. 2, but for run D (which assumes the interaction of nonspherical winds with different degree of asymmetry but with density $n \propto F_\theta$ in the pre-eruptive wind; see Table 1 and eq. [1]). Stratifications of the temperature (top left), density (top right), pressure (bottom left) and velocity-field (bottom right) computed for run D at $t = 160$ yr after the main eruptive event in the η Car wind. Given the latitude-variations (in both density and velocity) of the pre-eruptive wind, the equatorial features obtained from this scenario are very faint.

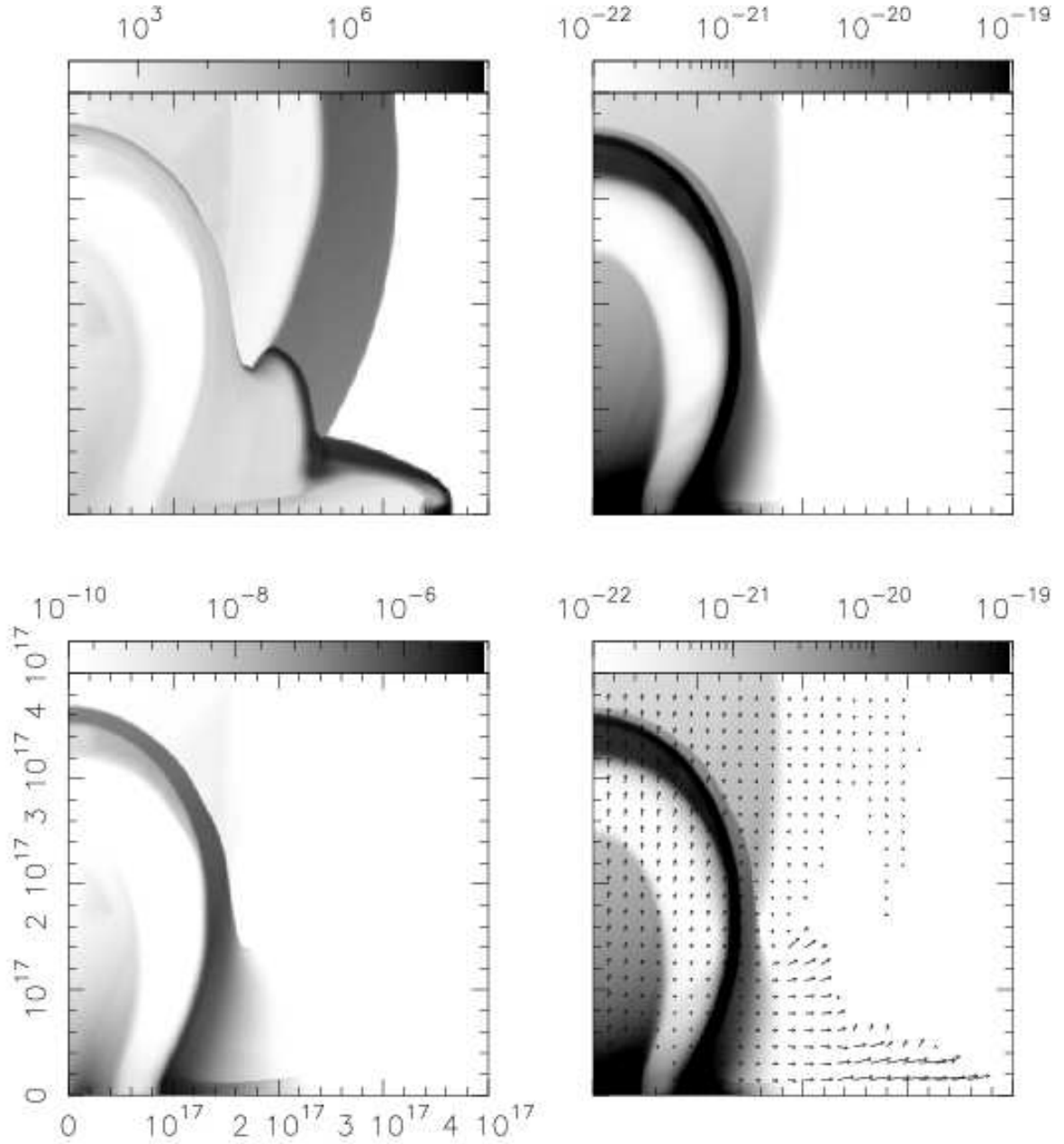


Fig. 6.— The same as Fig. 2, but for run E (which assumes the interaction of non-spherical winds with different degree of asymmetry but with a faster pre-outburst wind than in run C; see Table 1). Temperature (top left), density (top right), pressure (bottom left) and velocity field maps (bottom right) after ~ 160 years of the great eruption are presented. It can be observed that a similar structure to the Homunculus is reproduced, however the equatorial skirt is fainter and slower than the obtained from run C.

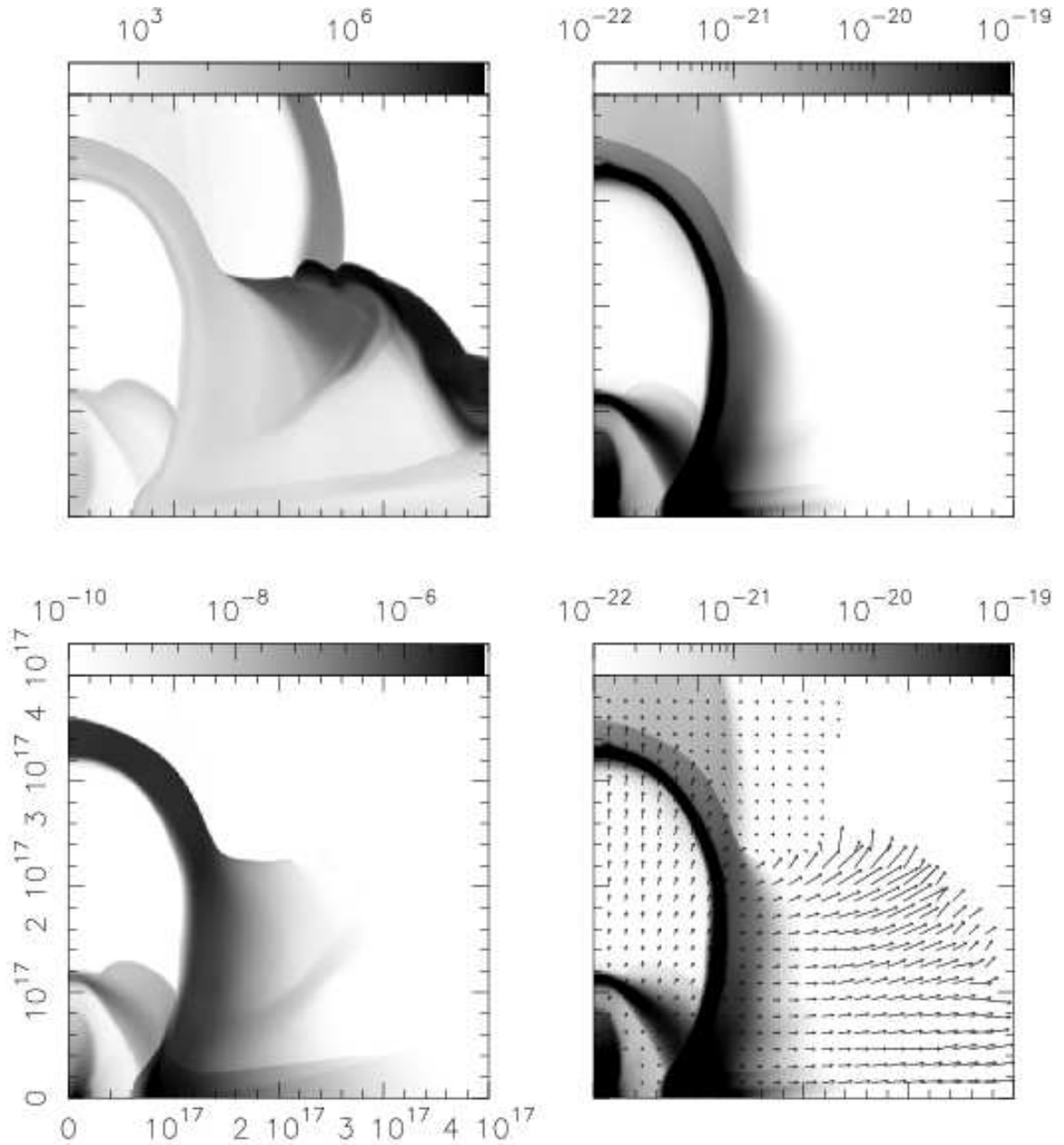


Fig. 7.— The same as Fig. 2, but for run F (which assumes the interaction between nonspherical pre-outburst and great eruption outflows with different degree of asymmetry, and includes a second spherical eruption; see Table 1). Temperature, density, pressure and velocity-field maps (top left, top right, bottom left and bottom right, respectively) for run E, at $t = 160$ yr of evolution after the great eruption. In this scenario, a second spherical eruptive event has been included showing the formation of an inner nebula (the little Homunculus). [This run has been presented also in Paper I.]

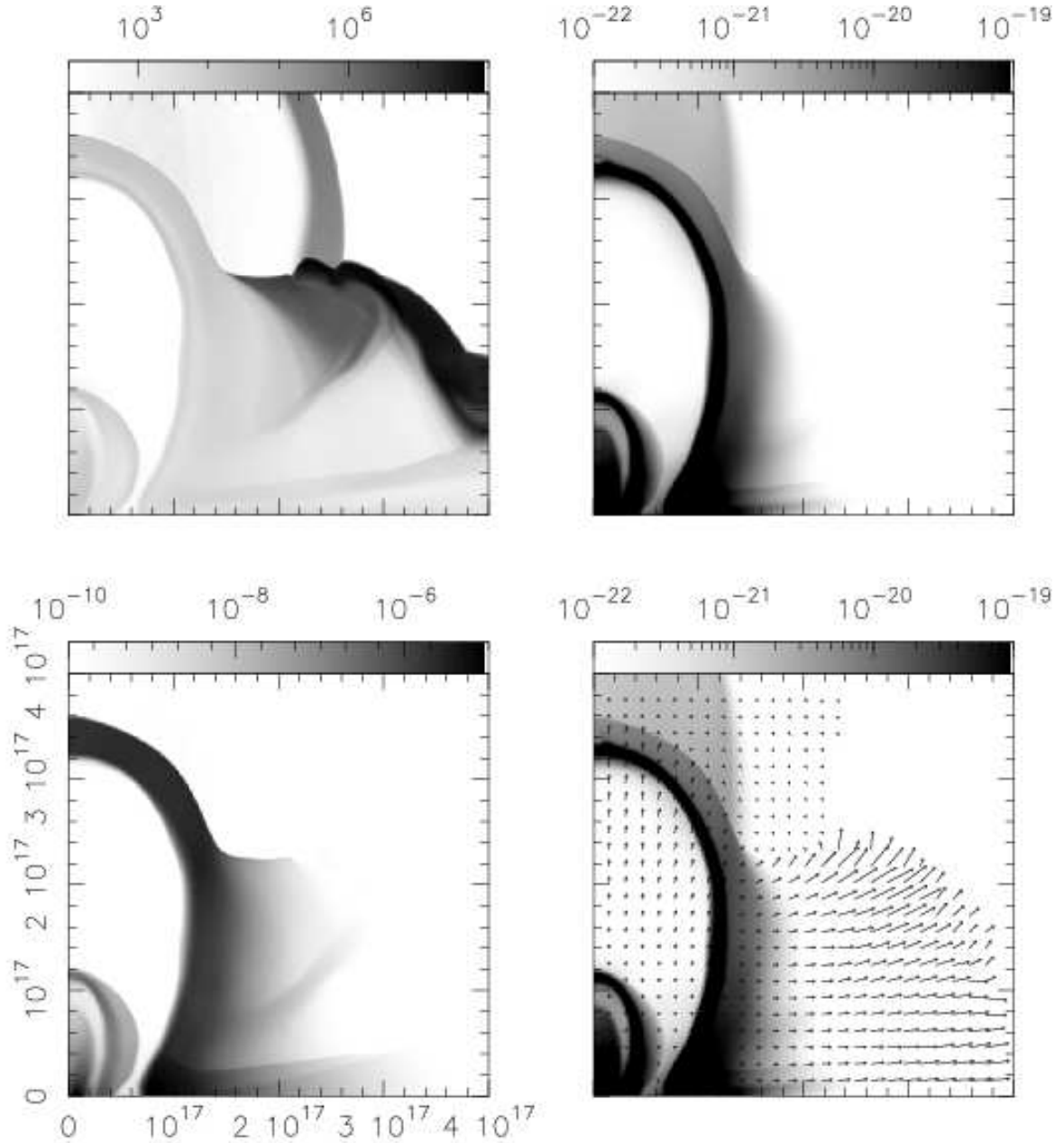


Fig. 8.— The same as Fig. 2, but for run G (which assumes the interaction between nonspherical pre-outburst and great eruption outflows with different degree of asymmetry, and includes a second nonspherical eruption; see Table 1). Stratifications of the temperature (top left), density (top right), pressure (bottom left) and velocity-field (bottom right) obtained from run F at $t = 160$ yr after the main eruptive event of η Car. This scenario includes a nonspherical ejecta (the minor eruption 50 yr after the great eruption) from which an inner nebula is also formed.

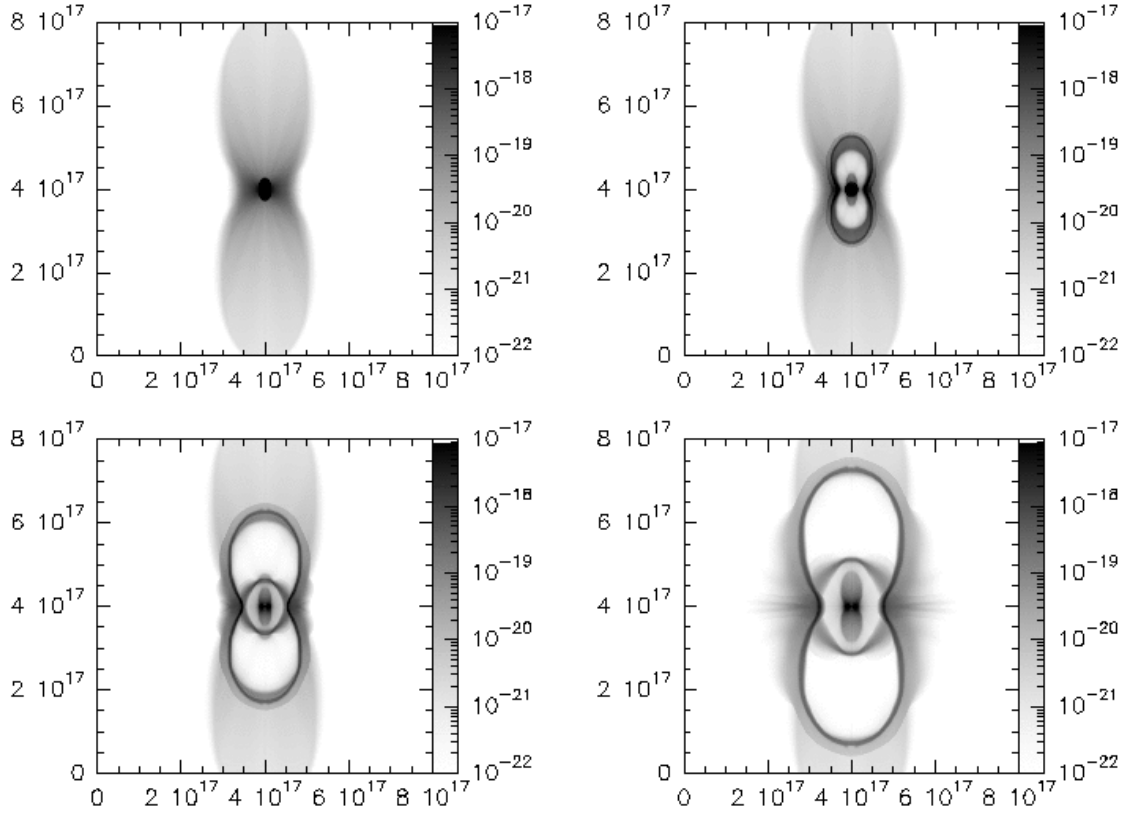


Fig. 9.— Log-scale density maps in four quadrants for four different times ($t = 10$ yr [top left], 60 yr [top right], 110 yr [bottom left] and 160 yr [bottom right]) in the evolution of the model of run F. The vertical scale of the density is in g cm^{-3} , and the x- and y-axes are in units of cm. This Figure is taken from Paper I.